Outflow of Arctic Ocean Sea Ice into the Greenland and Barents Seas: 1979–2007

R. KWOK

Jet Propulsion Laboratory, California Institute of Technology, Pasadena, California

(Manuscript received 2 September 2008, in final form 12 November 2008)

ABSTRACT

Twenty-nine years of Arctic sea ice outflow into the Greenland and Barents Seas are summarized. Outflow is computed at three passages: Fram Strait, between Svalbard and Franz Josef Land (S–FJL), and between Franz Josef Land and Severnaya Zemlya (FJL–SZ). Ice drift at the flux gates has been reprocessed using a consistent and updated time series of passive microwave brightness temperature and ice concentration (IC) fields. Over the record, the mean annual area outflow at the Fram Strait is 706(113) $\times 10^3$ km^2; it was highest in 1994/95 (1002 $\times 10^3$ km^2) when the North Atlantic Oscillation (NAO) index was near its 29-yr peak. The strength of the "Transpolar Drift Stream" (TDS) was high during the late 1980s through the mid-1990s. There is no statistically significant trend in the Fram Strait area flux. Even though there is a positive trend in the gradient of cross-strait sea level pressure, the outflow has not increased because of a negative trend in IC. Seasonally, the area outflow during recent summers (in 2005 and 2007) has been higher ($> 2\sigma$ from the mean) than average, contributing to the decline of summer ice coverage. Without updated ice thickness estimates, the best estimate of mean annual volume flux (between 1991 and 1999) stands at ~2200 km^3 yr^{-1} (~0.07 Sv: Sv $\equiv 10^6$ m^3 s^{-1}). Net annual outflow at the S–FJL passage is 37(39) $\times 10^3$ km^2; the large outflow of multiyear ice in 2002–03, marked by an area and volume outflow of 141 $\times 10^3$ km^2 and ~300 km^3, was unusual over the record. At the FJL–SZ passage, there is a mean annual inflow of 103(93) $\times 10^3$ km^2 of seasonal ice into the Arctic. While the recent pattern of winter Arctic circulation and sea level pressure (SLP) has nearly reverted to its conditions typical of the 1980s, the summer has not. Compared to the 1980s, the recent summer SLP distributions show much lower SLPs (2–3 hPa) over much of the Arctic. Overall, there is a strengthening of the summer TDS. Examination of the exchanges between the Pacific and Atlantic sectors shows a long-term trend that favors the summer advection of sea ice toward the Atlantic associated with a shift in the mean summer circulation patterns.

1. Introduction

In this paper, we provide an updated and expanded 29-yr view of the Arctic sea ice outflow into the Greenland and Barents Seas. This adds to the record of Fram Strait ice flux reported in Kwok and Rothrock (1999, hereafter KR99) and Kwok et al. (2004), and to the estimates of ice flux into the Barents Sea (Kwok et al. 2005). The examination of ice outflow bears on two problems: the mass balance and ice volume of the Arctic sea ice cover, and the potential impact of this freshwater on the Atlantic meridional overturning circulation. Accelerated changes in the Arctic ice cover and climate have made these topics increasingly compelling.

Indicators of Arctic Ocean sea ice cover (area and thickness) point to a recent decline in these variables. Since the early 1980s, a gradual decline in sea ice extent (3.7% decade^{-1}) can be seen in the satellite passive microwave analyses (Parkinson and Cavalieri 2008). The ice coverage set record lows during the summers of 2005 and 2007 (Comiso et al. 2006, 2008). The consequence has been reduced replenishment of the total multiyear ice area at the end of each summer (Kwok 2007), decreasing the coverage of thick, old ice and thus the survivability of the ice cover. The trend in multiyear ice coverage of the Arctic Ocean is, in fact, more negative than that of sea ice extent (Comiso 2002). The winter multiyear sea ice coverage in 2006 stood at ~50% of the Arctic Ocean area compared to the coverage of ~70% two decades ago. Analysis of sea ice draft from submarine cruises that cover a large part of the Arctic Ocean shows that there has been a decrease of 1.25 m in ice thickness during the period between

Corresponding author address: R. Kwok, MS 300-235, Jet Propulsion Laboratory, California Institute of Technology, 4800 Oak Grove Drive, Pasadena, CA 91109-8001.
E-mail: ron.kwok@jpl.nasa.gov

DOI: 10.1175/2008JCLI2819.1

© 2009 American Meteorological Society

1975 and 2000 (Rothrock et al. 2008). Evidence points to a depletion of the total Arctic sea ice volume and suggests substantial changes in the mass budget of the Arctic Ocean sea ice cover. Even though ice export is recognized as a key component of the annual mass balance, its role in the recent declines in sea ice coverage and volume is not readily apparent owing to our limited knowledge of the time variations in ice thickness distribution of the ice cover.

Outside the Arctic basin, anomalous inflows of Arctic sea ice are significant contributors to the freshening of the surface waters of the Greenland and Labrador Seas. Observations indicate substantial freshening of the northern North Atlantic from 1965 to 1995 (Curry et al. 2003; Curry and Mauritzen 2005), linked in part to increasing sea ice melt and export (Peterson et al. 2006). Studies have also suggested that the strength of the meridional overturning circulation is linked to these events through the impact of increased stratification on convective overturning (Dickson et al. 1988; Aagaard and Carmack 1989; Steele et al. 1996; Belkin et al. 1998).

On a broader scale, the outflow of Arctic sea ice into the Greenland and Barents Seas is an important component of the Arctic freshwater cycle. Recent estimates by Serreze et al. (2006) show that the sea ice transport through Fram Strait accounts for approximately 25% of the freshwater export from the Arctic Ocean. Moreover, the Fram Strait ice export introduces large interannual variability to this element of the Arctic freshwater cycle. However, a multidecade assessment of change in the total Arctic Ocean freshwater storage in sea ice remains elusive due to a lack of adequate ice thickness data. The thickness estimates from satellite altimeters (Kwok and Cunningham 2008) hold promise, but these are rather short records.

Outflow of Arctic sea ice through other passageways is beginning to receive more attention. Recent estimates of ice export at the Svalbard and Franz Josef Land (S–FJL) passage (Kwok et al. 2005) highlight the significant variability and its contribution to Arctic ice balance even though the mean flux is small. A large outflow in 2003 (over a 10-yr record) was preconditioned by an unusually high concentration of thick perennial ice over the Nansen Basin at the end of the 2002 summer. As a result, the winter ice area flux, at 110×10^3 km^2, was not only unusual in magnitude but also remarkable in that >70% of the area was multiyear ice. The corresponding ice volume flux at ~340 km^3 was almost one-fifth of the ice flux through Fram Strait. Studies suggest that the Barents Sea Branch Water (BSBW) is partly freshened by the meltwater from sea ice exiting the Arctic Ocean into the Barents Sea (Aagaard and Woodgate 2001; Woodgate et al. 2001; Kwok et al. 2005).

The present note discusses the 29-yr record of the Fram Strait ice flux as well as ice flux through passageways into the Barents Sea. The previous record (1979–2002) is extended by six years, and the record of ice drift estimates at the flux gates has been reprocessed using a consistent and updated time series of passive microwave brightness temperature and ice concentration (IC) fields. This paper is organized as follows. Section 2 describes the location of the flux gates, the ice motion fields, and ancillary datasets used in the analysis. The primary ice motion fields used are those from the *Nimbus-7* Scanning Multichannel Microwave Radiometer (SMMR: October 1978 to August 1987), Defense Meteorological Satellite Program Special Scanning Microwave Imager (SSM/I: 1987 to present), and Advanced Microwave Scanning Radiometer for Earth Observing System (AMSR-E) radiometers. Summer ice motion derived from AMSR-E is new and is now used in our outflow calculations. The uncertainties of the ice motion and flux estimates are briefly reviewed. Section 3 focuses on the mean and variability of the outflow at Fram Strait. The impact of declines in ice concentration is examined. To understand the origins and the impact of the outflow of the Arctic ice cover, the exported sea ice is traced to its source regions. These trajectories allow us to examine the variability and strength of the Transpolar Drift Stream (TDS). Section 4 turns to the Arctic outflow through passageways, between Svalbard and Fraz Josef Land (S–FJL) and between Franz Josef Land and Severnaya Zemlya (FJL–SZ), into the Barents Sea. Section 5 discusses the net sea ice outflow into the Greenland and Barents Seas and considers how the outflows are related to changes in the sea ice circulation pattern in the Arctic Ocean and indices of atmospheric oscillations. The last section concludes the paper.

2. Motion fields, flux estimates, and ancillary data

To estimate the outflow of Arctic sea ice into the Greenland and Barents Seas, we compute the sea ice flux through the Fram Strait and the S–FJL and FJL–SZ passages (Fig. 1). The Fram gate is positioned along a ~400 km line (at roughly 81°N) across the strait between Antarctic Bay in northeast Greenland and the northwestern tip of Svalbard. The gates between Svalbard and Franz Josef Land and Franz Josef Land and Severnaya Zemlya span approximate distances of 295 and 417 km, respectively. More details are provided about these gates in later sections. Here, we describe the source and quality of the ice motion data, how the outflows are estimated and also the ancillary datasets used in our analysis. Since some of the following material is covered in detail in KR99 and Kwok et al. (2004)

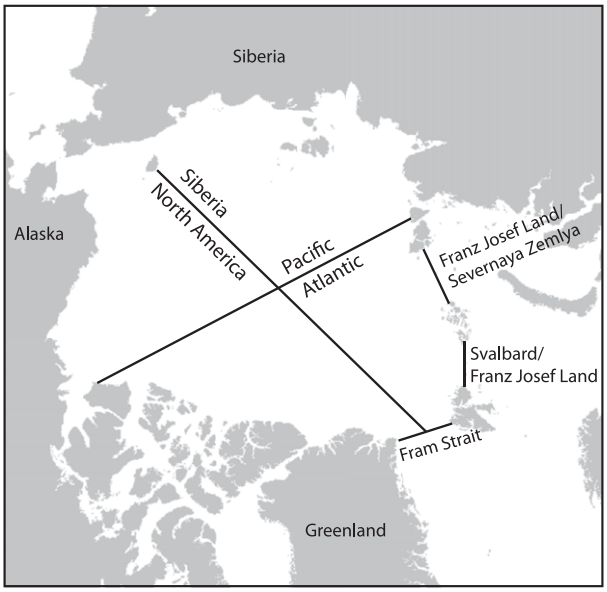

FIG. 1. Location of the five flux gates: Fram Strait, between Svalbard and Franz Josef Land, between Franz Josef Land and Severnaya Zemlya, between the Pacific and Atlantic sectors, and between the Siberian and North America sectors.

(especially the error analyses), the discussions here are brief.

a. Ice motion at the gates

Winter ice motion is derived from the daily brightness temperature fields acquired by the 89-GHz channel of the AMSR-E radiometer (2003–07), the 85-GHz channel of SSM/I (1992–2007), and the 2-day gridded fields from the 37-GHz channels of SMMR (1978–87) and SSM/I (1987–2007). The latest reprocessed brightness temperature fields from SSM/I radiometers are used (Maslanik and Stroeve 1990). The procedure for extraction of ice motion in the neighborhood of the flux gates is detailed in KR99. Based on comparisons with Synthetic Aperature Radar (SAR) and buoy drift, the uncertainties in the displacement vectors of the three channels are approximately 10 km (37 GHz), 5–6 km (85 GHz), and 3 km (89 GHz). For a more detailed description of the assessment of these uncertainties, the reader is referred to KR99.

Even though the winter ice motion from the 85- and 89-GHz channels are of better quality because of their higher spatial resolution (12.5 and 6.25 km, respectively), only the combined motion estimates from the 37-GHz channels of SMMR and SSM/I span the entire 29-yr period between 1979 and 2007. The consistency of the 37-GHz time series is thus better suited for examination of the multidecadal variability of Arctic ice flux. We include the estimates from the higher-resolution sensors primarily for assessment of the relative differences during the latter part of the record when there are overlapping motion estimates.

Summer ice motion at the flux gates is from the 18-GHz channel of the AMSR-E radiometer. The summer ice tracking approach is described in Kwok (2008). The improved spatial resolution of this channel (~25 km), with its lower sensitivity to atmospheric moisture compared to the 36-GHz channel, seems to have alleviated various issues that have plagued summer motion retrievals from shorter wavelength observations. The uncertainty of the summer displacement vectors from the 18-GHz channel, at ~3–4 km, is comparable to that of the quality of the winter displacements. The approaches for estimating both winter and summer ice flux are described below.

b. Flux estimates

Winter (October–May) area flux (F) is the integral of the product between the gate-perpendicular component of the motion (u) and ice concentration (C) along the gate. It is computed using the trapezoidal rule:

$$F = \sum_{1}^{N-1} 0.5(u_i + u_{i+1}) C_i \Delta x. \tag{1}$$

Here N is the number of points along the gate. The motion profile is constrained to go to zero, within a narrow zone of ~10 km, at the coastal endpoints. If we assume that the errors of the motion samples are additive, unbiased, uncorrelated, and normally distributed, the uncertainties in the area flux over any given time step σ_F can be computed; namely (KR99),

$$\sigma_F = \sigma_u L / \sqrt{N_s}, \tag{2}$$

where L is the width of the flux gate, σ_u is the uncertainty in the displacement estimates over the time step, and N_s is the number of independent samples across the gate; N_s is based on the number of nonoverlapping windows used in the calculation of ice drift across a gate.

The uncertainty in average winter area flux estimates σ_T, again assuming that the errors in the n-day area flux are additive, unbiased, uncorrelated, and normally distributed, can be written as

$$\sigma_T(\mathrm{km}^2) = \sigma_F \sqrt{N_D}, \tag{3}$$

where N_D is the number of observations over the period of interest. We do not expect these errors to be correlated since individual area flux estimates are derived from temporally distinct passive microwave fields. Between October and May, there are approximately 240 daily flux estimates and half as many 2-day estimates. For Fram Strait, these equations give uncertainties in

TABLE 1. Expected uncertainties (σ_T) in the winter (October–May) area flux across the three gates. Here σ_u is the n-day displacement uncertainty and N_s is the number of independent motion estimates across the gate.

		2 day 37 GHz (σ_u = 10 km)		1 day 85 GHz (σ_u = 6 km)		1 day 89 GHz (σ_u = 3 km)	
Gate	Width	N_s	σ_T (10^3 km^2)	N_s	σ_T (10^3 km^2)	N_s	σ_T (10^3 km^2)
Fram Strait	410	3	25	5	17	10	6
S–FJL	295	2.5	20	4	14	8	6
FJL–SZ	417	3	26	5	17	10	6

the winter area flux σ_T of approximately 17×10^3 km^2 if we use the daily 85-GHz estimates compared to 25×10^3 km^2 using the 2-day 37-GHz estimates. This amounts to ~4% of the average winter Fram Strait area flux of about 616×10^3 km^2. Table 1 shows the winter flux uncertainties for this and the other gates.

Summer ice export during the SMMR and SSM/I years is treated differently because the drift estimates from low-resolution passive microwave observations are unreliable due to the effects of atmospheric moisture and surface melt. Previously, for Fram Strait, we have used a rough linear relationship between monthly ice area flux and cross-strait sea level pressure gradient (ΔP) from the winter to estimate summer ice flux (Kwok et al. 2004). Here, we have refined the regression coefficients based on five years of daily summer ice area flux from the 18-GHz channel of AMSR-E (see Fig. 2). We use these new coefficients to estimate the daily area flux for the days between June and September. Regression analysis shows that the daily ΔP explains ~60% of the variance in the Fram Strait area flux with an error of $\sim 1.0 \times 10^3$ km^2. After accounting for the additional uncertainty in daily AMSR-E ice flux estimates of $\sim 0.7 \times 10^3$ km^2 [Eq. (2) with σ_u = 3 km and $N_s = 3$], we obtain a net daily uncertainty of 1.1×10^3 km^2. Applying Eq. (3) with $\sigma_F = 1.1 \times 10^3$ km^2 and $N_D = 120$ (four months of summer) we obtain an uncertainty in the 4-month (June–September) summer Fram Strait area flux of $\sim 12 \times 10^3$ km^2. This can be compared to the mean summer flux estimate of 91×10^3 km^2. Summing [in a root-sum-square (RSS) sense] the uncertainties for winter and summer gives an annual (October–September) uncertainty of $\sim 28 \times 10^3$ km^2. Following this procedure, we compute the regression coefficients for the other gates and their associated uncertainties. The uncertainties in the summer, winter, and annual (October–September) area flux for the three gates are shown in Table 2.

To summarize, the 29-yr record of winter (October–May) ice flux is computed from 37-GHz ice motion from SSMR and SSM/I. In the summer, AMSR-E ice motion fields are used during the years when they are available (2003–07); otherwise, the ice flux is derived using the coefficients from the regression analysis described above.

c. *Ancillary datasets*

In KR99, ice concentration inside the ice edge is taken as 100% and is not used in computing ice area flux because of the large uncertainties in IC and the shorter record. Since there is a significant negative trend in Arctic ice extent and area of ~4% decade^{-1} (Comiso and Nishio 2008) over the entire passive microwave record of >29 yr, we feel it is essential to capture these trends in our calculation of area flux. In Eq. (1), we use the IC time series from a recent dataset constructed by Comiso and Nishio (2008). To maintain consistency in their ice concentration estimate throughout the SSM/I and SMMR records, their brightness temperature fields are first normalized to be consistent with those from AMSR-E before an identical retrieval algorithm is used to derive sea ice parameters from the three datasets. As we show in the next section, the trend in ice concentration is significant at Fram Strait, especially during the winter months. It is also important to note that

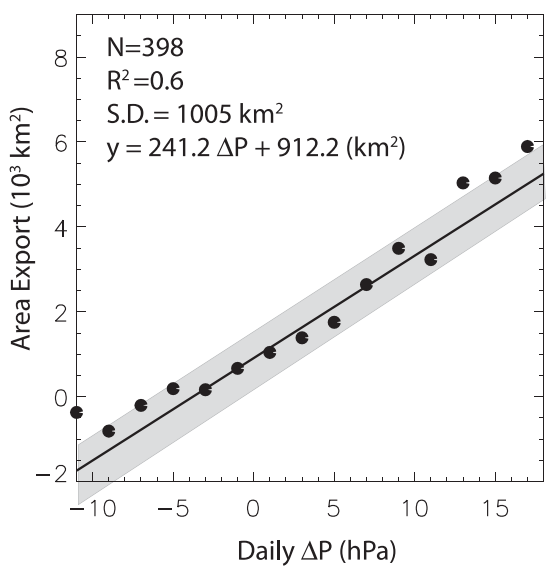

FIG. 2. Regression of the daily Fram Strait ice flux from AMSR-E and the cross-strait gradient of sea level pressure. Each symbol in the plot represents the mean of all samples within a 2-hPa bin. Uncertainty of regression (1σ) is shown in gray.

TABLE 2. Expected uncertainties (σ_T) in the summer (June–September) and net (summer and winter) area flux across the three gates. The mean annual ice area flux at these gates is shown for comparison. Only 1-day 85-GHz ice motion is used at the FJL–SZ gate. Positive (negative) sign indicates Arctic outflow (inflow).

Gate	Width	Summer σ_T (10^3 km^2)	Winter σ_T (10^3 km^2)	Annual σ_T (10^3 km^2)	Annual mean (10^3 km^2)
Fram Strait	410	13	25	28	706
S–FJL	295	7	20	21	37
FJL–SZ	417	6	17 (85 GHz)	19	−103

uncertainty in ice concentration could be up to several percent, and it varies seasonally with the highest values in the summer. In the winter Arctic, the daily uncertainties are approximately 4%–7% with possible biases of similar magnitude (Cavalieri 1992). This adds to the uncertainty in our flux calculations.

3. Fram Strait outflow

In this section, we first assess the relative consistency of the ice flux estimates from the SMMR, SSM/I, and AMSR-E radiometers; summarize the variability of area outflow over the 29-yr record; and then examine the time-varying strength of the Transpolar Drift Stream. We will provide a brief remark on the volume flux. Regarding our terminology and sign convention, outflow (positive) refers to export of Arctic sea ice while inflow (negative) refers the import of sea ice into the Arctic Ocean.

a. Comparison with estimates from 85-GHz SSM/I and 89-GHz AMSR-E channels

As mentioned earlier, the 29-yr record is derived from the 37-GHz channel of the SMMR and SSM/I radiometers. To assess the relative consistency of the estimates, the latter years of this record can be compared to the better-quality flux estimates from the higher-resolution 85-GHz SSM/I (1992–2007) and 89-GHz AMSR (2003–07) channels. The annual outflows from the three records are compared in Fig. 3. It can be seen that the three time series of annual outflows are highly correlated. The mean and standard deviation (shown within parentheses) of the differences between the channels are $-28.0(40.0) \times 10^3$ km^2 (37 versus 85 GHz); $0.0(39.0) \times 10^3$ km^2 (37 versus 89 GHz); and $-3.0(20.0) \times 10^3$ km^2 (89 versus 85 GHz). Between the 37-GHz and 85/89-GHz channels the standard deviations are similar, while the differences between the two higher-resolution channels are lower. These differences are relatively small

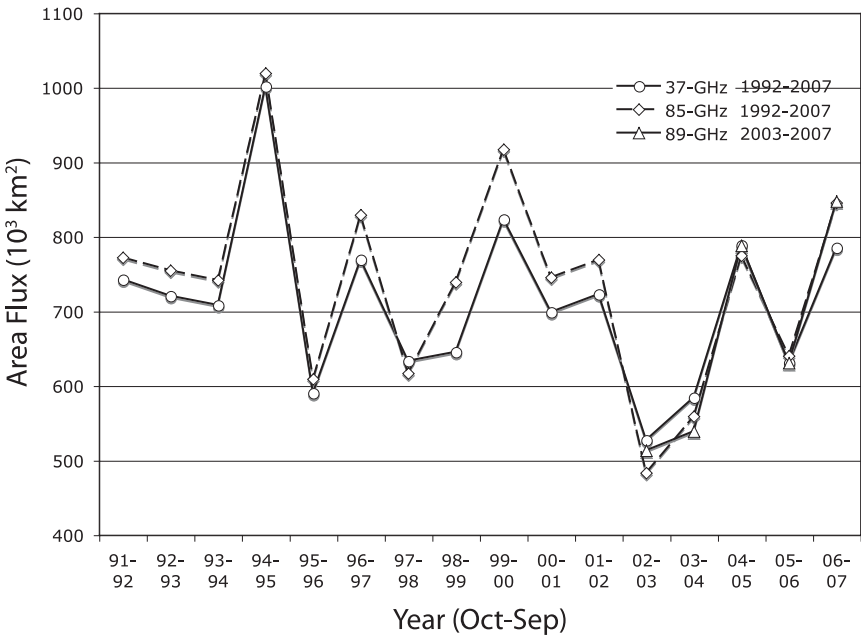

FIG. 3. Comparison of the annual (October–September) Fram Strait area flux estimates from the 37-GHz SSM/I, 85-GHz SSM/I, and 89-GHz AMSR-E radiometer channels.

TABLE 3. Mean (standard deviation in parentheses) annual, summer and winter, and highest and lowest Arctic sea ice outflow/exchanges at the following gates (10^3 km^2).

Outflow	Annual mean (std dev)	Winter mean (std dev)	Summer mean (std dev)	Highest annual (yr)	Lowest annual (yr)
Fram Strait	706 (113)	616 (92)	91 (34)	1002 (1994–95)	516 (1984–85)
S–FJL	37 (39)	30 (36)	7 (9)	141 (2002–03)	−23 (1993–94)
FJL–SZ	−103 (93)	−109 (90)	6 (20)	73 (1997–98)	−285 (1999–2000)
Pacific–Atlantic	588 (323)	389 (262)	199 (171)	1192 (1994–95)	45 (1984–85)
Siberia–North America	263 (223)	227 (150)	36 (114)	585 (2005–06)	−320 (1997–98)

(<5%) compared to the large mean and variability of the ice area flux at the Fram Strait (Table 3).

b. Interannual and seasonal variability

Instead of over a calendar year, we define our annual Arctic sea ice outflow as the net over a 12-month period between October and September; this is a better measure of the behavior during a seasonal cycle of growth and melt. Figure 4 shows the variability of the annual, seasonal, and monthly Arctic area export through the Fram Strait (F). In particular, the normalized monthly anomalies in Fram Strait outflow

$$\widehat{F}_m = \frac{F_m - \bar{F}_m}{\sigma_{F_m}}$$

are shown in Fig. 4b, where $\bar{F}_m$ and σ_{F_m} denote the 29-yr monthly means and standard deviations.

Over the 29-yr (1979–2007) record, the average annual IC-weighted outflow is 706(113) $\times$ 10^3 km^2—the sum of an average winter (October–May) and summer (June–September) contribution of 616(92) $\times$ 10^3 km^2 and 91(34) $\times$ 10^3 km^2, respectively (summarized in Table 3). Quantities within parentheses are standard deviations. Overall, the area flux is reduced by ~10% when it is weighted by ICs. The mean seasonal cycle (Fig. 4a) shows the highest flux during December and March. The four months of summer explain only ~13% of the annual average. There is significant interannual variability: the annual area flux ranges from a minimum of 516 $\times$ 10^3 km^2 in 1984–85 to a peak of 1002 $\times$ 10^3 km^2 in 1994–95. During these two extremes, Fig. 4b shows the monthly outflow to be anomalously high (red) for nearly all months during 1994–95 and, similarly, anomalously low (blue) for nearly all months during 1984–85.

There is no statistically significant trend in the annual Fram Strait outflow. The small positive trend in the shorter 18-yr record (1978–96) reported by KR99 is likely a result of the bias introduced by the large ice outflow in 1994–95 near the tail of that time series. In fact, the outflow for that year remains the highest over the longer record. It is interesting to note, however, that the outflow during the past summers (in 2005 and 2007) has been remarkably high. The ice flux during the summer of 2005 was 144 $\times$ 10^3 km^2 but the flux in 2007, at 167 $\times$ 10^3 km^2 (>2σ from the mean), is the highest on record and accounted for over 20% (compared to an average of 13%) of the 2006–07 annual outflow. Figure 4b shows three months (June, August, and September) of anomalously high (red) outflow in 2007. As discussed in a later section, this has implications on the mass balance of the Arctic Ocean sea ice.

c. Trends in ice concentration and cross-strait pressure gradient

We reiterate that, in the present analysis, we have weighted the area flux with ice concentration while we have not done so in earlier publications (e.g., KR99). Therefore, the outflows are somewhat lower. The trends in the monthly ice concentration and ice extent at the Fram Strait flux gate are shown in Figs. 5a and 5b. The ice extent is that fraction of the flux gate covered by sea ice (with ice concentration > 15%) and is an indication of the width of the ice stream at the flux gate. Except for the near zero trends in IC in September and October, negative trends are seen in all months, with the largest trend during the summer month of July (−7.4% decade^{-1}). Similarly, except for the same two months, the monthly trends in ice extent are also negative indicating a narrowing of the ice stream especially during the latter half of the record; there are more open water areas covering the flux gate east of Svalbard.

Why are the negative trends in ice concentration/extent not seen in the annual ice area flux? To answer this, we plot the trends in monthly mean cross-strait sea level pressure gradient (ΔP in Fig. 5c) to examine this proxy of wind forcing at the Strait. Northerly winds or drainage of sea ice from the Arctic Ocean is associated with positive gradients (ΔP). Interestingly, the trend in ΔP is positive for all months with the largest positive trends during the months of January, February, and March. The results seem to indicate that negative trends in the ice concentration—a reduction in ice area—have provided a rough balance of the overall positive trend in ΔP.

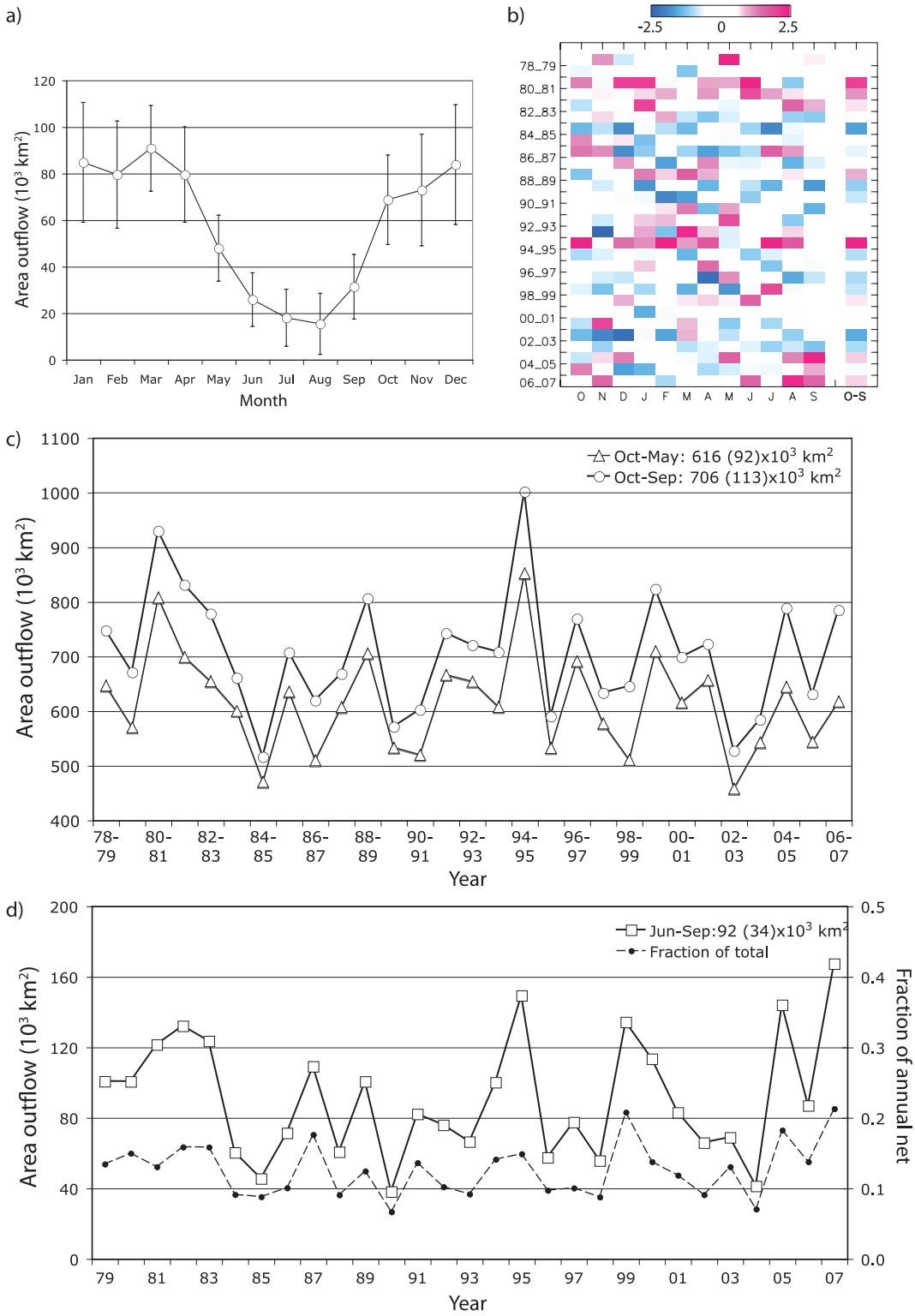

FIG. 4. Arctic sea ice outflow through Fram Strait (1978–2007). (a) Seasonal cycle. (b) Normalized monthly anomalies (see description in section 3b). (c) Winter (October–May) and annual (October–September) outflow. (d) Summer outflow and as fraction of net annual export. Quantities within parentheses are standard deviations.

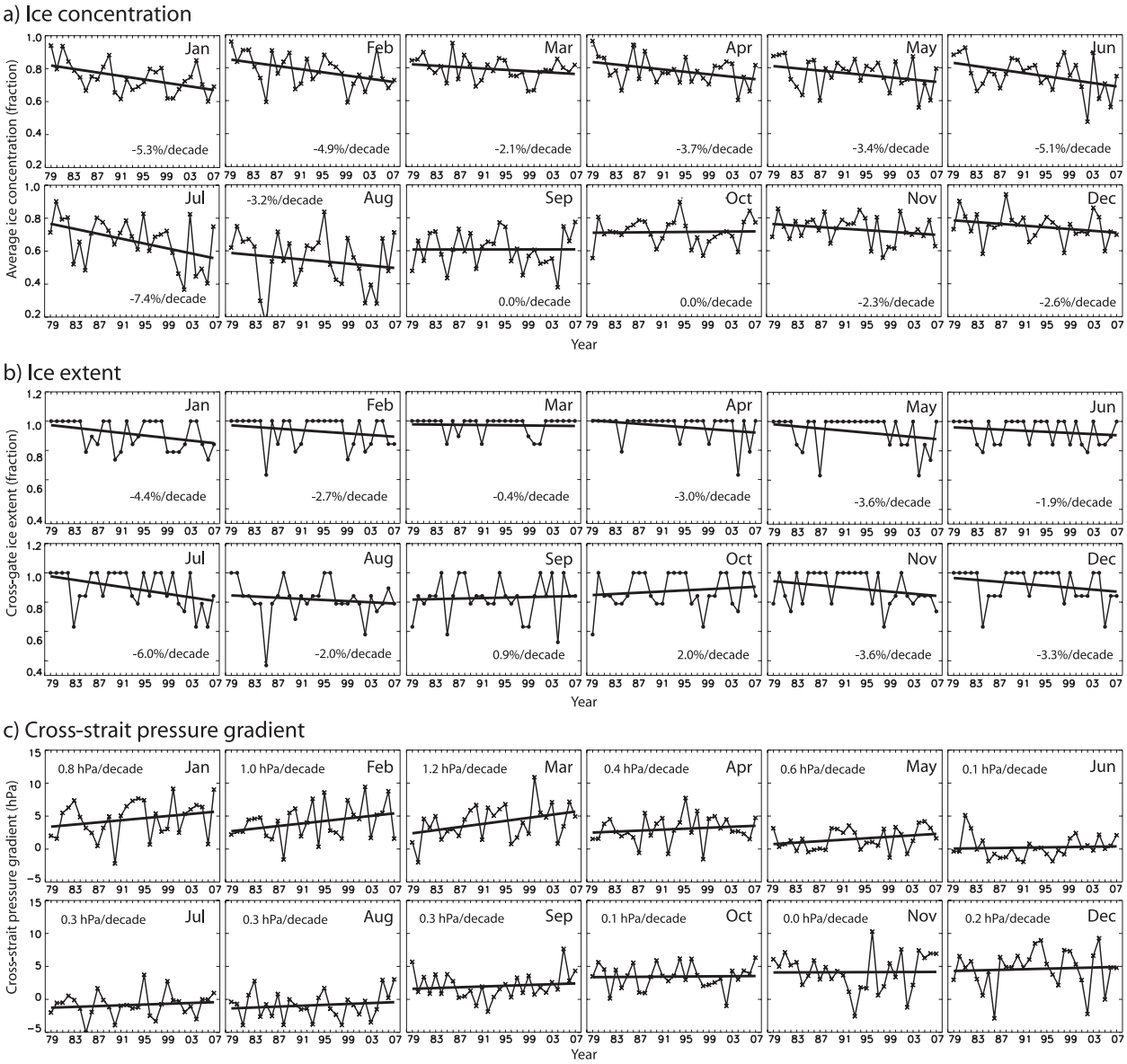

FIG. 5. Trends in (a) average monthly ice concentration across the Fram Strait flux gate, (b) the fractional extent of the gate covered by sea ice (>15% ice concentration), and (c) cross-strait sea level pressure gradient (ΔP) between 1979 and 2007.

d. Transpolar Drift Stream and Arctic ice export

To identify the source regions of sea ice exported through Fram Strait, we construct the trajectory of ice particles during the 12 months prior to their crossing the Fram Strait flux gate in April (end of winter). These are constructed by backpropagation of ice particles at the gate using optimally interpolated motion fields of the Arctic Ocean (Kwok 2000). The results for the 29 years are shown in Fig. 6. The expanse of coverage of the Arctic Ocean swept by these trajectories shows the strength, preferred orientation, and width of the TDS for that particular year. Extent of contributions to the outflow can be seen in the depth of penetration and expanse of the Arctic Ocean covered by the isochrones of ice locations (in color).

For describing the variability of the TDS, we define its axis to be that line joining the endpoints of the trajectory that crosses the center of the flux gate (shown in black in Fig. 6). The length of the line provides a measure of the net displacement of an ice particle at the center of the flux gate, and the orientation of the TDS axis serves as an indication of whether the source of sea ice, for that particular season, is the Eastern (Siberian)

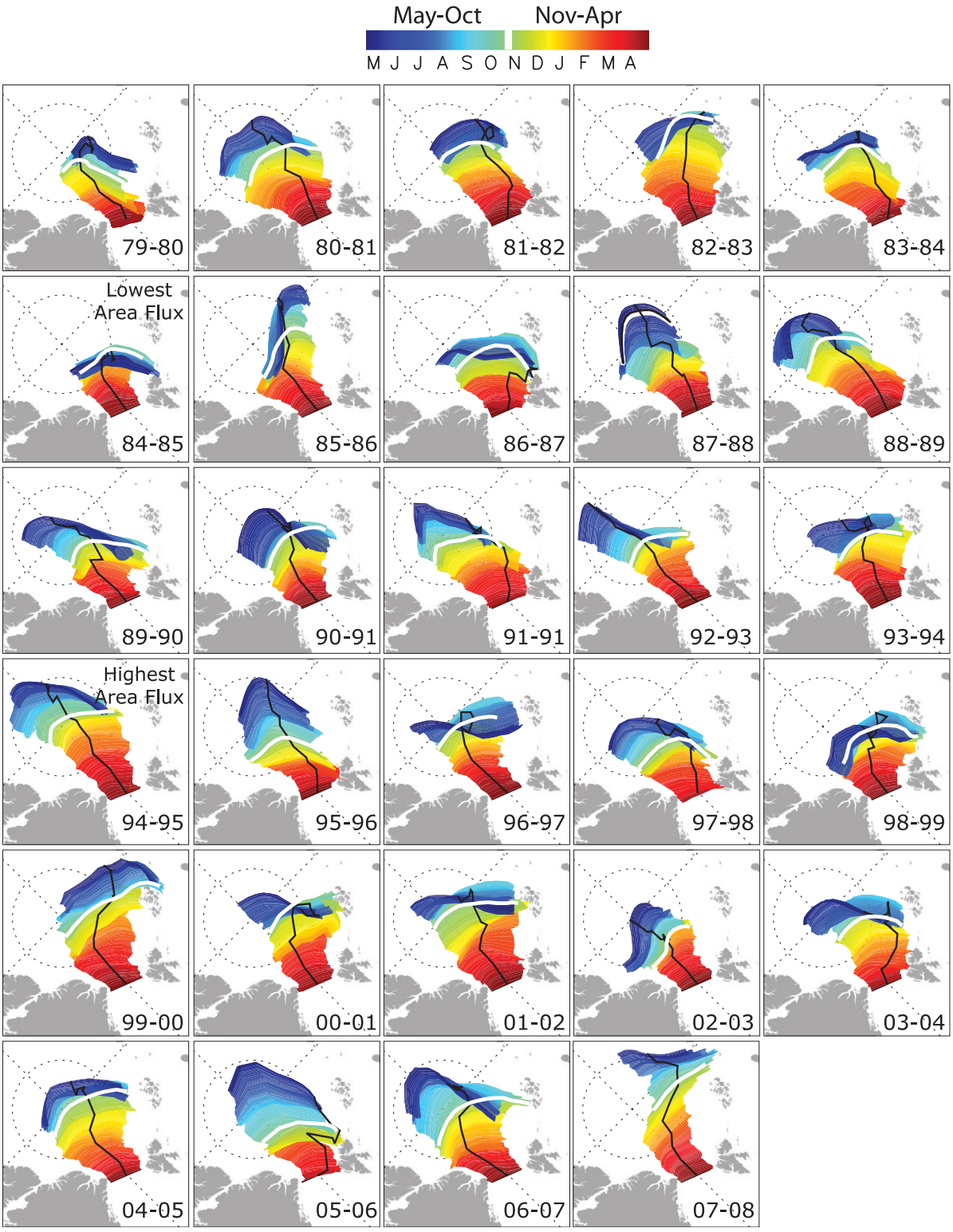

FIG. 6. Character of the TDS as depicted by the trajectory of ice particles over a 12-month period prior to their crossing the Fram Strait flux gate in April. A black line joining the endpoints of a trajectory defines the axis of the TDS for a given year. The white line at the center of the color scale divides the 12-month period in half. Isochrones (in color) show the trajectory of the particles defining the flux gate before they exit Fram Strait.

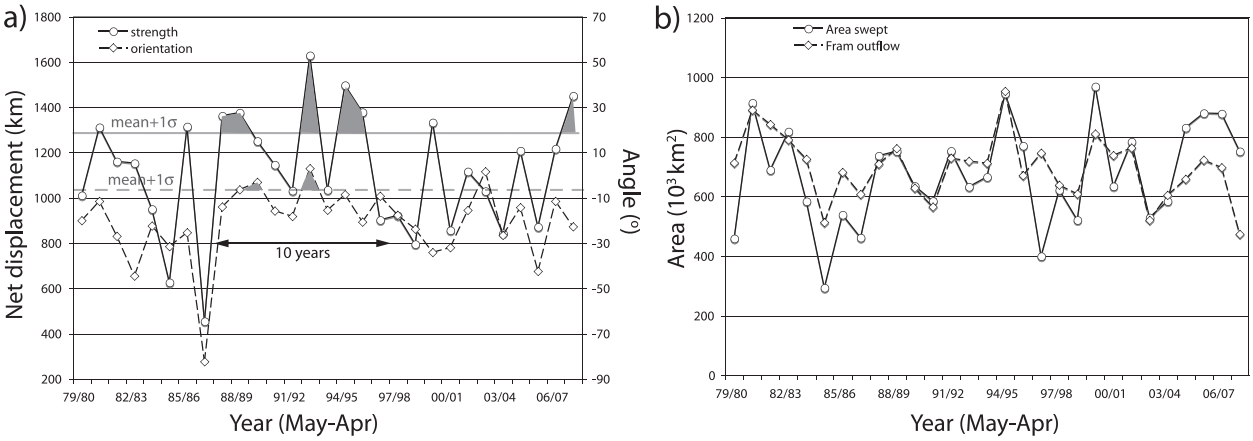

FIG. 7. (a) Net displacement of ice particles at the center of the flux gate and the axis of the TDS relative to that of the prime meridian (east is negative and west is positive). Gray lines show mean plus one standard deviation from the mean for the two parameters. Shaded areas show unusually high displacements and orientation angles during the 10 yr indicated in the plot. (b) Comparison of annual area export at Fram Strait with the area swept by the particle trajectories.

or Western (North American) Arctic. The angular orientation of this axis is measured relative to that of the prime meridian (with east negative and west positive). We also calculate the total area swept by the trajectories during their 12 months of transit from its axis source location to the flux gate. This provides a measure of the area exported through the Strait. These attributes of the TDS are plotted in Fig. 7.

The average length of the axis is 1100 (270) km and ranges from 454 km (1986–87) to 1630 km (1992–93) (Fig. 7a). Quantities within parentheses are standard deviations. For comparison, the distance from Fram Strait to the North Pole is less than 1100 km. The average net displacement of >130 km month^{-1} (mean plus one standard deviation) in 1992–93 points to a strong TDS. At this average drift rate, it takes less than two years for sea ice to transit the Arctic Ocean from the coast of Siberia to Fram Strait. In fact, the drift of the *Tara* (Gascard 2008) does not seem all that unusual compared to recent conditions, but the contrast is certainly remarkable relative to the drift of the *Fram*. The mean orientation of the axis is −21°(15°) and varies between −82° (1986–87) to 3° (1992–93). When the axis is tilted toward the west (i.e., positive), thicker/older ice from the Beaufort Sea and north of Greenland typically feeds the TDS. In the other extreme, an eastward-tilting axis usually indicates that the sea ice is likely thinner/younger, as that ice originates from the seasonal ice cover and is closer to the summer ice edge (Kwok et al. 2004). In terms of the area swept by the trajectories (Fig. 7b), the mean is 676(169) × 10^3 km^2 and the area ranges from 295 × 10^3 km^2 (1984–85) to 969 × 10^3 km^2 (1999–2000). This mean value can be compared to the average Fram Strait outflow of 706 × 10^3 km^2. The relatively high correlation between the time series of annual area export at Fram Strait and the area swept by the particle trajectories can be seen in Fig. 7b. The difference and correlation between the two time series are −20(139) × 10^3 km^2 and 0.58, respectively.

In 1992–93, the combined strength of the TDS (trajectory length of 1629 km, the highest on record) and the extreme westward tilt of its axis (3°) likely contributed to the export of a significant volume of thick ice even though the Fram Strait area outflow that year did not exceed that of the peak year of 1994–95. In the year with the largest area export (1994–95), the North Atlantic Oscillation (NAO) index was at a near record (29 yr) high (close to 4), and the ice velocities at Fram Strait were the highest because the positioning of the Icelandic low favored ice export.

While there is no discernible trend in strength and orientation, it is interesting to note the extremes in these two TDS attributes occurred within the 10 yr between 1987 and 1996. During this period, there are 5 yr where the net displacements of the ice particles within the TDS are more than one standard deviation above the mean (samples above the solid and dashed gray lines in Fig. 7a). This points to a period of high ice flux with orientation angles that favor the drainage of sea ice from the western Arctic Ocean and north of Greenland, that is, export of thicker sea ice.

The possible impact of this potentially large volume flux is discussed in Lindsay and Zhang (2005). They hypothesized that the increased thinning rate of Arctic sea during 1988–2003 was due to a gradual warming of the Arctic over the last 50 years leading to reduced first-year ice thickness at the onset of melt together with a shorter-term increase in export of thick multiyear ice associated

with changes in circulation patterns of the Arctic Oscillation in the late 1980s and early 1990s. The consequences have been increases in the area of summer open water allowing increased heating of the ocean, creating a positive feedback scenario that favors additional thinning of the ice cover. Our record of ice export and strength of the TDS during this period between 1987 and 1996 certainly lends credence to their hypothesis that these years of high ice flux may have played a significant role in accelerating the decline of the Arctic Ocean sea ice cover.

e. Remarks on volume flux

By combining area export and 8 yr (1991–99) of ice draft measurements from moored upward looking sonars (ULS) south of Fram Strait, Kwok et al. (2004) estimated the mean annual flux for the period to be ~2200(500) km^3 (or ~0.07 Sv: Sv $\equiv 10^6$ m^3 s^{-1}). The annual flux ranges from 1790 km^3 yr^{-1} to 3360 km^3 yr^{-1}. Over the period, the ULS ice thickness shows an overall decrease of 0.45 m in the mean ice thickness and a decrease of 0.23 m over the winter months (December through March). Correspondingly, the mode of the multiyear ice thickness distributions exhibits an overall decrease of 0.55 m and a winter decrease of 0.42 m. This shorter record seems consistent with the decrease of 1.25 m in ice thickness that Rothrock et al. (2008) estimated using the longer 25-yr record (1975 and 2000) of submarine ice draft of mostly the central Arctic Ocean.

If the ice cover had continued to thin after 2000 and since there is no trend in the ice area flux, then we would expect the annual volume export to decrease. But beyond 2000, ice draft observations from Fram Strait are no longer available in the public archive. This represents a serious data deficiency in an area of critical interest to studies in Arctic climate and hydrology. Even though satellite-derived ice thicknesses hold promise and are becoming available (Kwok and Cunningham 2008), it is not clear that they will be able to provide, in the short term, a consistent time series, when compared to the moored ULS data, for the observation of trends in thickness and export at Fram Strait.

4. Arctic sea ice outflow into the Barents Sea

In this section, we discuss the outflow of Arctic sea ice at the two passages: 1) S–FJL and 2) FJL–SZ. The latter passage is actually connected to both the Kara Sea as well as the Barents Sea.

a. Passage between Svalbard and Franz Josef Land

The 295-km S–FJL flux gate is between Storøya, Svalbard, and Zemlya Alekandry, Franz Josef Land. A 10-yr record (1994–2003) of winter outflows of Arctic sea ice into the Barents Sea is reported in Kwok et al. (2005). Here, the length of that record is extended to 29 years.

1) Comparison with estimates from 85-GHz SSM/I and 89-GHz AMSR-E channels

As with the Fram Strait estimates, we assess the relative differences of the S–FJL outflow between the 37-GHz channel of the SMMR and SSM/I radiometers and those from the higher-resolution 85-GHz SSM/I (1992–2007) and 89-GHz AMSR-E (2003–07) channels. The agreement between annual Arctic outflows from the three records can be seen in Fig. 8a. The mean and standard deviation of the differences between the channels are $-0.0(33.0) \times 10^3$ km^2 (37 versus 85 GHz); $15.0(33.0) \times 10^3$ km^2 (37 versus 89 GHz); and $-2.0(9.0) \times 10^3$ km^2 (37 versus 85 GHz). Even though the three time series are highly correlated, it should be noted that the differences are relatively large compared to the much lower average annual outflow of $37(39) \times 10^3$ km^2 (Table 3).

2) Interannual and seasonal variability

Figures 8b and 8c show the variability of the seasonal and annual S–FJL area export of Arctic sea ice over the 29-yr (1979–2007) record. The average annual outflow is $37(39) \times 10^3$ km^2, with average contributions of $30(36) \times 10^3$ km^2 and $7(9) \times 10^3$ km^2 during the winter (October–May) and the summer (June–September), respectively (summarized in Table 3). The mean seasonal cycle (Fig. 8b) shows higher flux over the winter, with a distinct minimum during August. The four months of summer explain about one-fifth of the annual ice flux. The IC-weighted annual area flux ranges from a minimum of -23×10^3 km^2 in 1993–94 to a peak of 141×10^3 km^2 in 2002–03. There are net inflows, albeit small, into the Arctic Ocean during some years.

There is no statistically significant trend in the S–FJL Arctic sea ice outflow over the record. Except for the large area outflow during the winter 2002/03, the outflows in other years are relatively low—only ~5% when compared to the Fram Strait area export. The large area outflow in 2003 ($>2\sigma$ from the mean) was associated with a deep atmospheric low situated over the eastern Barents Sea that winter; the strong northerly winds associated with this arrangement in sea level pressure distribution pushed the ice southward over the Arctic Ocean toward the Barents Sea. Together with the presence of an unusually high concentration of thick multiyear ice over the Nansen Basin (near the flux gate) at the end of the 2002 summer (Kwok et al. 2003), the result was a remarkable outflow of Arctic sea ice volume (340 km^3—~15% of the Fram flux) that year. In contrast, 2002–03 was one of the lowest years of area export (527×10^3 km^2) at Fram Strait. This was also

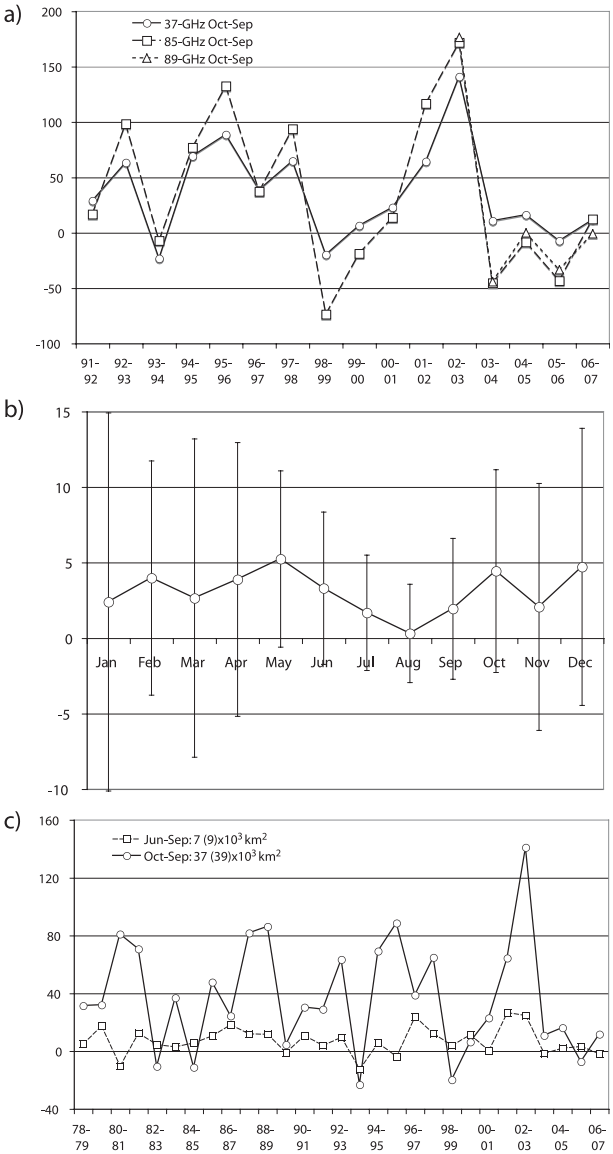

FIG. 8. Outflow of Arctic sea ice through S–FJL: (a) Comparison of the annual (October–September) outflows from the 37-GHz SSM/I, 85-GHz SSM/I, and 89-GHz AMSR-E radiometer channels, (b) seasonal cycle, and (c) net annual (October–September) and summer (June–September) outflows. Quantities within parentheses are standard deviations.

associated with the unusual pressure distribution over the Barents and Greenland Seas.

b. *Passage between Franz Josef Land and Severnaya Zemlya*

Two gates cover the 417-km opening into the Barents and Kara Seas: one between Franz Josef Land and Ushakova and the other between Ushakov and O Pioner on Severnaya Zemlya. The ice export estimates use ice drift from the 85-GHz channel and the record covers a shorter period between 1992 and 2007. Prior to 1992, the ice motion estimates are not reliable owing to the ice conditions and the lower resolution of the SSM/I radiometer.

1) COMPARISON WITH ESTIMATES FROM THE 89-GHZ AMSR-E CHANNELS

The mean and standard deviation (within parentheses) of the differences between the channels are $-8.0(12.0) \times 10^3$ km^2 (89 versus 85 GHz). This can be compared to the mean area flux of $-103(93) \times 10^3$ km^2 (negative for inflow). The agreement between annual outflows from the two records can be seen in Fig. 9b.

2) INTERANNUAL AND SEASONAL VARIABILITY

The seasonal and annual variability of the Arctic outflow at the FJL–SZ gate is shown in Fig. 9. Over the 15-yr (1992–2007) record, the average annual area flux is $-103(93) \times 10^3$ km^2. The negative sign indicates a net annual inflow of sea ice into the Arctic Ocean through this passageway. This represents the sum of an average winter (September–May) and summer (June–September) contribution of $-109(90) \times 10^3$ km^2 and $6(20) \times 10^3$ km^2, respectively (summarized in Table 3). As we show in the drift patterns (Fig. 10), the Kara Sea in addition to the Barents Sea seem to be source regions of sea ice for the Arctic Ocean. The mean seasonal cycle (Fig. 9) shows the highest inflow between December and February. Compared to net Arctic import during the winter, there seems to be negligible exchange of sea ice through this gate in the summer. As the standard deviation in ice transport is comparable to the mean, the interannual variability is significant. The IC-weighted annual area flux ranges from a minimum of -285×10^3 km^2 in 1999–2000 to a peak of 73×10^3 km^2 in 1997–98. We find no statistically significant trend in FJL–SZ area outflow over the record.

5. Linkages to atmospheric indices, Arctic sea ice circulation, and regional exchanges

a. *Linkage of Fram ice export to AO and NAO*

Variability of the Arctic ice export over the 29-yr record can be linked to changes in sea ice thickness and changes in large-scale atmospheric circulation associated with the Arctic Oscillation (AO) (Thompson and Wallace 1998) and the North Atlantic Oscillation (NAO) (Hurrell 1995). The squared correlation between the NAO and AO indices is 0.71. The correlations between ice flux and these indices indicate a connection between the variability in the Arctic ice outflows and the larger-scale atmospheric oscillations. For this 29-yr record, the squared correlation between the

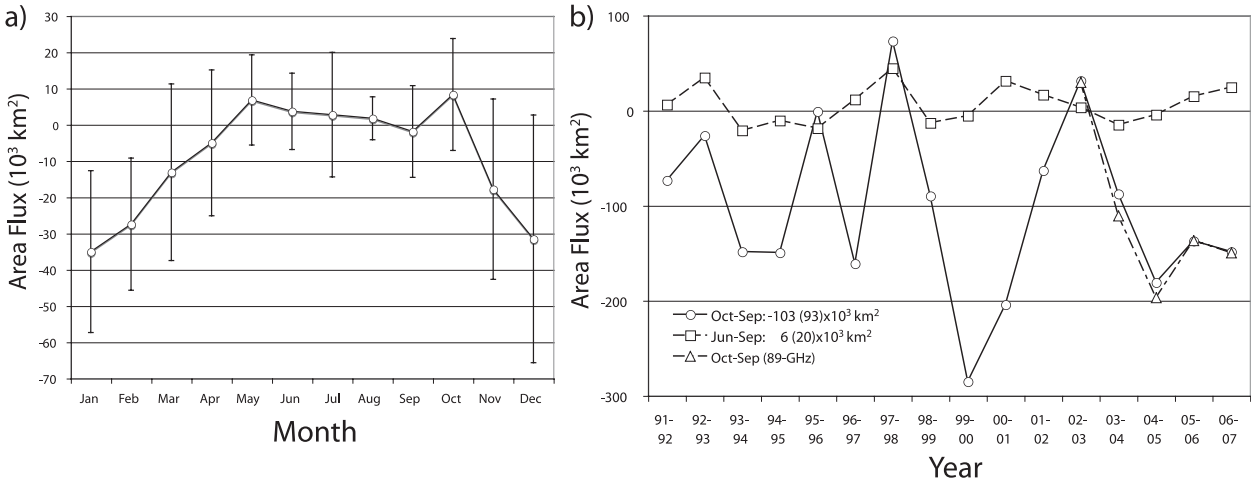

FIG. 9. Arctic sea ice outflow through FJL–SZ: (a) Seasonal cycle. (b) Net annual (October–September) and summer (June–September) outflows and comparison with export estimates from the 89-GHz AMSR-E radiometer channels. Quantities within parentheses are standard deviations.

December–March (DJFM) Fram Strait area export and NAO index is 0.36 and is 0.28 for the AO index. This can be compared to a squared correlation of 0.44 and 0.39 obtained from the 18-yr and 24-yr time series reported in KR99 and Kwok et al. (2004). Potentially, the higher correlations of the shorter time series (in KR99) could have been due to the coincidence of that record with the extreme positive phase of the AO and NAO during the late-1980s until the mid-1990s. The correlation values are higher when the years with negative NAO and AO indices are excluded. This suggests that, during the negative phases, Fram Strait fluxes may be associated with a different mode of variability or a shift in position of the common features of the North Atlantic circulation pattern that affect Arctic sea ice export. Other investigators (Hilmer and Jung 2000; Vinje 2001), using model simulations and ice flux parameterizations, have also suggested that the link between ice area flux and the indices of the AO and NAO is more tenuous, and the connection may be less robust during the negative phases of the AO and NAO. Nevertheless, the results here suggest that the correlation of the ice export with these indices remains significant.

b. Connections to Arctic sea ice circulation

To examine the Arctic ice flux and the near-decadal variability of the sea ice circulation within the Arctic Ocean, we divide the 29-yr period into three regimes relative to their DJFM AO and NAO indices: 1) the first neutral regime—R1 (1979–87); 2) the second high/positive regime—R2 (1988–96); and 3) the last neutral regime—R3 (1997–2007). As discussed in the previous sections, the second regime (R2) features higher-than-normal winter sea ice flux coupled with a strong TDS when compared to R1 and R3. The mean summer and winter sea ice circulation patterns and sea level pressure distribution for the three regimes are shown in Figs. 10a,b,c,g,h,i. Also shown are the winter and summer differences between the three regimes (R2 minus R1, R3 minus R2, and R3 minus R1). A similar analysis of the response of sea ice to the Arctic Oscillation, for the years between 1979 and 1998, can be found in Rigor et al. (2002).

The winter sea ice motion (IM) patterns and sea level pressure (SLP) distribution in R3 (Fig. 10c) suggest that both of these fields have nearly reverted from their cyclonic state in R2 (Fig. 10b) to the anticyclonic state characteristic of R1 (Fig. 10a). The shift of the TDS axis toward the western Arctic from R1 to R2, and then back during R3, can be clearly seen. The interregime difference fields illustrate these changes. Between R1 and R2 (Fig. 10d), there is a general decrease in SLP (up to 5 hPa) over a large part of the Arctic Ocean (dashed isobars) associated with the positive phases of the AO/NAO. The vector differences show increases in ice velocities through Fram Strait. The features of the R1 to R2 changes have been discussed in Rigor et al. (2002). From R2 to R3 (Fig. 10e), a return to a more neutral AO/NAO state is seen in the increase in SLP over most of the Arctic. In fact, except for the sign, the difference SLP and ice motion patterns are almost identical to those changes observed between R1 and R2. Finally, the near reversion to the R1 state over R3 is clearly evident in Fig. 10f: the difference SLP pattern is quite flat and the difference ice motion vectors, except for those near Fram Strait, are small. Morison et al. (2007) also observed that Arctic circulation had nearly reverted to

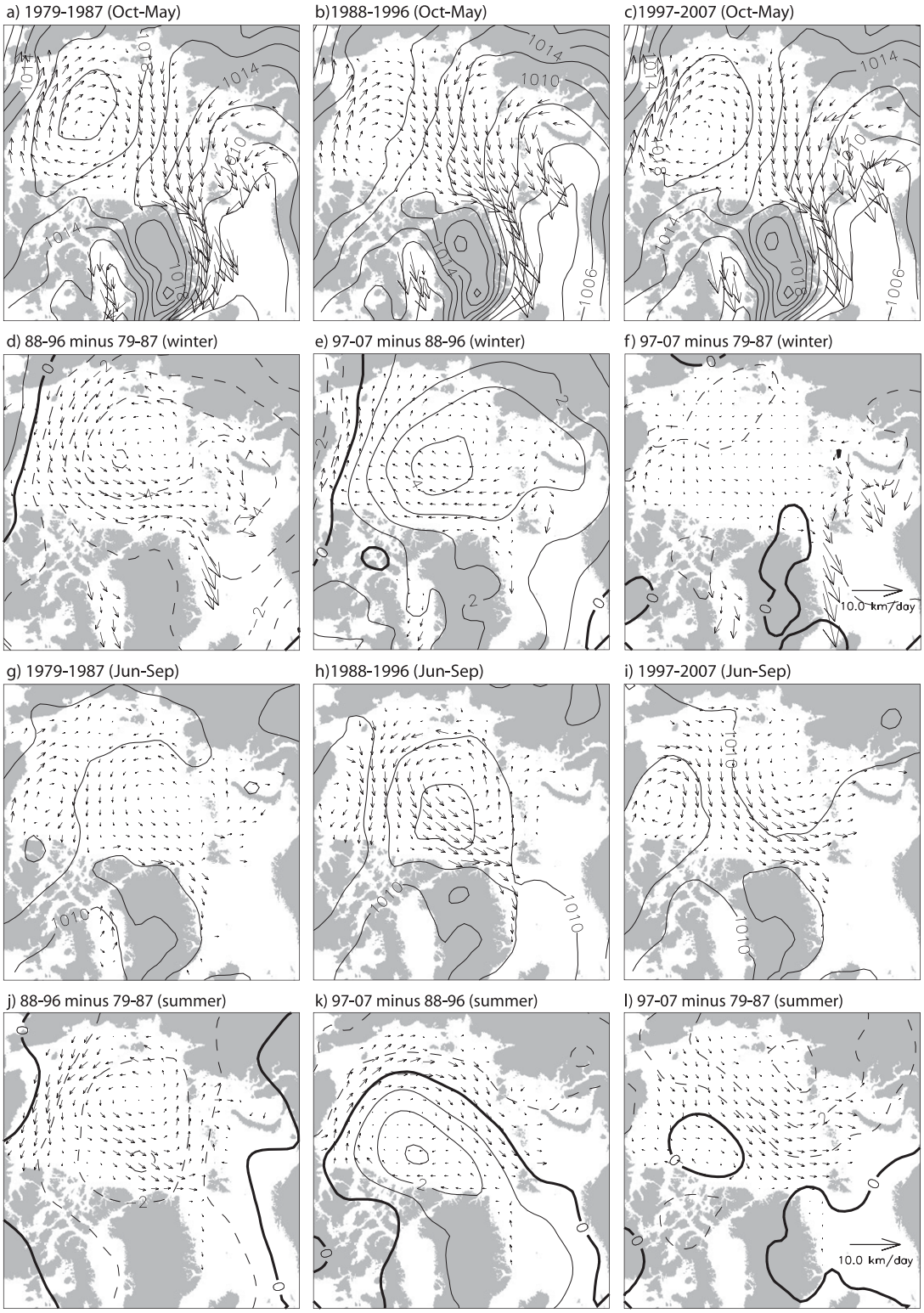

FIG. 10. Changes in the mean sea ice circulation and sea level pressure distributions during three periods: 1979–87, 1988–96, and 1997–2007. (a),(b),(c) The mean winter (October–May) fields. (d),(e),(f) The winter difference fields. (g),(h),(i) The mean summer (June–September) fields. (j),(k),(l) The summer difference fields. The zero difference isobar is in bold and positive (negative) difference isobars are shown as solid (dashed) lines. (Contour intervals: 2 hPa for the mean fields and 1 hPa for the difference fields.)

conditions typical of the 1980s. The large ice vectors at Fram Strait are associated with the positive trend in the cross-strait pressure gradient between Greenland and Svalbard discussed earlier (Fig. 5c).

The summer SLP and ice circulation patterns exhibit some of the same behavior as those of the winter fields. In R1 (Fig. 10g), the mean IM/SLP fields show a relatively weak cyclonic pattern throughout the Arctic Ocean. In contrast, a much stronger cyclonic circulation associated with deeper low can be seen in R2 (Fig. 10h). The intensity of the low (~2 hPa) can be seen in Fig. 10j. This generally lower SLP over the Arctic Ocean seems to be correlated with the winter behavior in R2. With the shift of the characteristic summer low SLP pattern from the central Arctic (in R2) toward the Taymyr Peninsula (in R3), there is higher pressure over the central Arctic (Fig. 10k). This shift in the mean atmospheric pattern seems to have tilted the axis of TDS toward the Siberian coast, with the mean IM predominantly offshore in this sector of the Arctic Ocean. Broadly speaking, this is also similar to that of the behavior in winter. However, the summer R3–R1 field (Fig. 10l) does not show a near reversion to the R1 state as do the winter fields. Compared to R1, the summer interregime difference shows a much lower pressure (2–3 hPa) over much of the Arctic. Together, a stronger TDS is seen in both R2 and R3. This changes our notion of relatively weak SLP gradients that generally prevail during the summer. In the next section, we show that there are positive trends in the time series of summer regional transport of sea ice from the Pacific to the Atlantic sectors. Since the AO/NAO indices capture primarily the SLP pattern and variability of the cold season, segmenting the 29 summers into the three regimes (as above) based on these indices may not isolate the behavioral modes of the summer circulation patterns. In any case, the three regimes highlight the contrast between summer and winter behavior and their time variations.

c. *Regional sea ice exchanges*

Here, we examine the regional exchanges within the Arctic Ocean to see how they relate to basin-scale circulation patterns (discussed above) and the ice outflow at the gates into the Barents and Greenland Seas. Kwok (2008) estimated the exchange of sea ice between the Pacific and Atlantic sectors and found that the relatively large advection of sea ice into the Atlantic sector during the summers of 2006 and 2007 was associated with the record minimums in summer ice extents and above-average ice export at Fram Strait. This is further explored in the longer 29-yr record. Although it is not unexpected that the transport of sea ice from the Pacific to the Atlantic sectors via the TDS is the primary conduit of sea ice to Fram Strait, it would be interesting to examine the variability of regional and seasonal exchanges of sea ice associated with changes in circulation within the Arctic Ocean.

We define two gates (see Fig. 1) to examine the large-scale exchanges of sea ice within the Arctic Ocean. A line connecting the southwestern tip of Banks Island and the easternmost tip of Severnaya Zemlya (2840 km in length) divides the Arctic into the Pacific and Atlantic sectors (P and A sectors), and serves as the gate where area exchanges are calculated. The second flux gate, a line from Wrangel Island across the Arctic to the center of Fram Strait (3100 km), divides the Arctic Ocean into the Siberia and North America sectors (S and NA sectors). The ice flux is calculated as in Eq. (1). In our sign convention, exports from the Pacific to the Atlantic and from Siberia to North America are positive. Figure 11 summarizes the interannual, annual, and seasonal area exchanges at the two flux gates, and Fig. 12 shows the normalized monthly anomalies.

1) EXCHANGE BETWEEN THE PACIFIC AND ATLANTIC SECTORS

Over the 29-yr (1979–2007) record, the net exchange of sea ice between the P and A sectors is 588(323) $\times$ 10^3 km^2—the sum of an average winter (October–May) and summer (June–September) contribution of 389(262) $\times$ 10^3 km^2 and 199(171) $\times$ 10^3 km^2, respectively (Table 3). There is net outflow from the P to the A sector. As there is no distinct seasonal cycle as in the other gates (Fig. 11c), the four months of summer account for about one-third of the annual average. There is significant interannual variability: the annual area flux ranges from a minimum of 45 $\times$ 10^3 km^2 in 1984–85 to a peak of 1192 $\times$ 10^3 km^2 in 2006–07. The normalized monthly anomalies (Fig. 12a) show that the area exchange between the sectors is anomalously high for nearly all months during 2006–07. The exchange during the summer of 2006–07 is the highest on record. Similarly, anomalously low exchanges are seen for nearly all months during 1984–85. The squared correlations between the detrended DJFM exchange of sea ice area between the P and A sectors and the Fram Strait outflow, AO, and NAO are 0.35, 0.25, and 0.12, respectively. The wintertime series explains more than a third of the winter sea ice export at Fram Strait.

The mean seasonal profiles along the gate (Fig. 11d) show the predominant anticyclonic (clockwise) and cyclonic (counterclockwise) circulation of the Arctic during the winter and the summer (Fig. 10). Associated with winter high pressure patterns over the Canada Basin, there is net advection of sea ice from the P to the

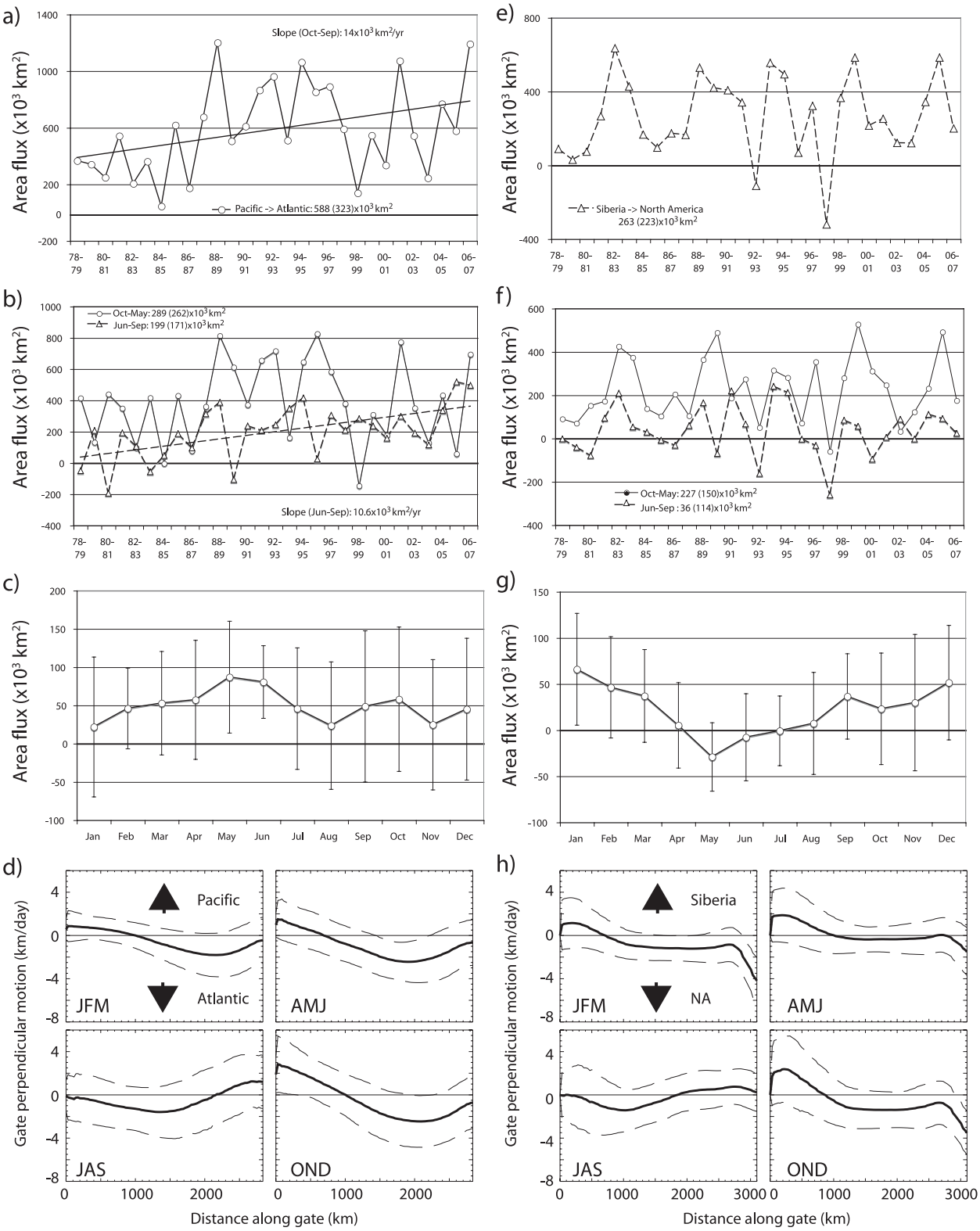

FIG. 11. Area exchanges at the Pacific–Atlantic and Siberia–North America flux gates shown in Fig. 1: (a),(e) Net annual flux; (b),(f) winter and summer outflows and their trends; (c),(g) seasonal cycle; (d),(h) flux profiles. Quantities within parentheses are standard deviations.

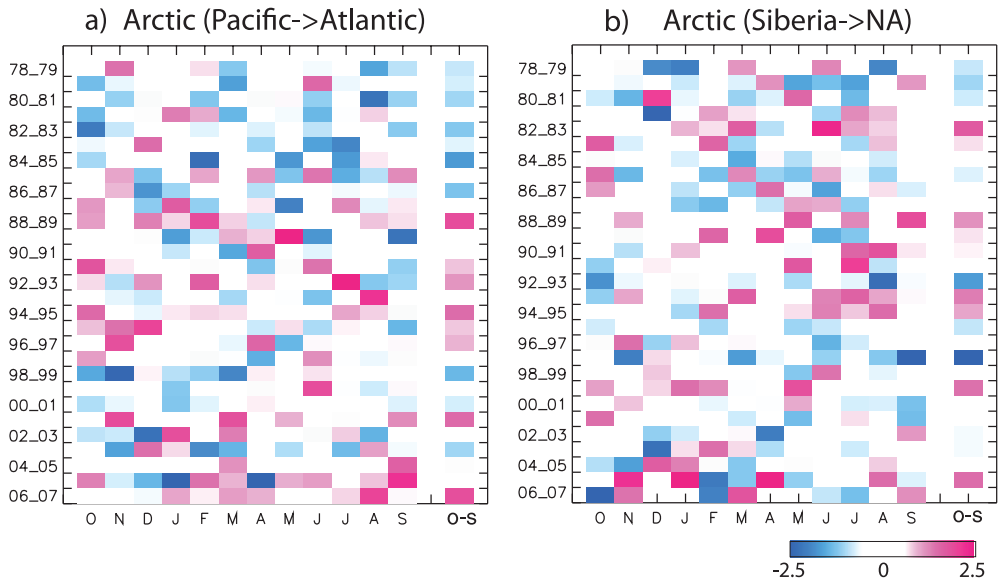

FIG. 12. Normalized monthly area exchanges (see description in section 3b) at the Pacific–Atlantic and Siberia–North America flux gates.

A sector in the eastern Arctic side of the gate compared to a more moderate return flow in the western Arctic end of the gate. The summer circulation associated with the low pressure pattern over the eastern Arctic shows a profile with its trough shifted toward the central Arctic.

Similar to the extremes in the strength and orientation of the TDS, the winter transfer of sea ice from the P sector (Fig. 11b) was higher during the 10 yr between 1987 and 1996. Again, during this period, there are 5 yr where the net outflow is $>1\sigma$ above the mean. There is a statistically significant trend of 14×10^3 km^2 yr^{-1} in the annual exchanges between these sectors. The increase in summer (June–September) exchanges is responsible for a large fraction of the annual trend. Alone, the summer trend is 10.6×10^3 km^2 yr^{-1}. Over the 29 years, this trend suggests a remarkable increase from almost zero to more than 300×10^3 km^2 of sea ice export to the A sector during the summer (Fig. 11b). This is associated with the changes in the summer circulation pattern, as discussed in the previous section. The mean summer SLP and circulation patterns have changed in a manner (discussed above) that seems to favor a stronger summer TDS and net export of sea ice from the P to the A sectors. This is a source of sea ice for export through Fram Strait. The average Fram Strait ice export during summer for the R2 and R3 regimes was higher in R1.

2) EXCHANGE BETWEEN THE SIBERIA AND NORTH AMERICA SECTORS

The mean net advection of sea ice between the S and NA sectors is $263(223) \times 10^3$ km^2, with an average winter (October–May) and summer (June–September) contribution of $227(150) \times 10^3$ km^2 and $36(114) \times 10^3$ km^2, respectively (Table 3). The net exchange favors the NA sector. The seasonal cycle shows the highest inflows into the NA sector during the winter months of November through March (Fig. 11g). The regional exchanges during four months of summer are small and explain only about 14% of the annual average. The annual area flux ranges from a minimum of -320×10^3 km^2 in 1997–98 to a peak of 585×10^3 km^2 in 2005–06. Inflows into the S sector occur mostly in the summer (Fig. 11f). The squared correlations between the detrended DJFM exchange of sea ice area between the S and NA sectors and the Fram Strait outflow, AO, and NAO are 0.17, 0.20, and 0.33, respectively. The effect of the NAO on the circulation of the Arctic ice is more significant at this gate and explains more than one-third of the S to NA sector exchanges.

Similar to the discussion above, the mean seasonal profiles along the gate (Fig. 11h) are expressions of circulation associated with the winter high and summer low pressure patterns over the Arctic Ocean. The westward drift of sea ice in the Beaufort Sea in winter dominates (Fig. 10) the first 1000 km of the profile. The next 1500 km is quite flat and is associated with the steady drift along the TDS before the sea ice picks up speed prior to drainage into the Greenland Sea through Fram Strait. In the summer, the ice motion toward the NA sector (Fig. 11h), associated with the prevailing low pressure pattern (Fig. 10), is more prominent while the Fram Strait feature seen in the

winter profiles is absent due to the small cross-strait SLP gradient.

There is no statistically significant trend in the annual exchanges between the S and NA sectors during the winter or summer. The S sector is a source of sea ice area for the NA sector. Unlike the P–A sector exchanges, the 10 yr between 1987 and 1996 do not stand out as being a period of remarkable transport over a background of the 29-yr time series. The interannual variability is comparable to the mean.

6. Conclusions

The present note summarizes 29 years of Arctic sea ice outflow into the Greenland and Barents Seas. The ice export is computed at three passages: Fram Strait, between Svalbard and Franz Josef Land (S–FJL), and between Franz Josef Land and Severnaya Zemlya (FJL–SZ). The motion at the flux gates has been reprocessed using a consistent and updated time series of passive microwave brightness temperature and ice concentration (IC) fields. The Fram Strait ice export is related to the strength of the Transpolar Drift Stream, the North Atlantic and Arctic Oscillations, sea ice circulation and regional sea ice exchanges within the Arctic Ocean. Here, we revisit and discuss some of the noteworthy points.

The mean annual (summer and winter), ice-concentration-weighted area outflow at Fram Strait is $706(113) \times 10^3$ km^2. There is no statistically significant trend in the Fram Strait area flux. The year 1994–95, when the NAO index was near its 29-yr peak, remains the one with the highest outflow (1002×10^3 km^2) on record. Even though there is a positive trend in the gradient of cross-strait sea level pressure, especially between January and March, the area outflow has not increased observably because of a negative trend in ice concentration. Due to the lack of ice thickness data after the year 2000, we have not been able to update our time series of volume flux. Our best estimate of the mean annual volume flux using satellite ice drift (between 1991 and 1999) remains at ~2200 km^3 yr^{-1} (~0.07 Sv) (Kwok et al. 2004). This short record, during a period of positive regime in the AO and NAO, does not allow us to assess the volume flux during years when the AO/NAO remained relatively neutral. Although the analysis of sea ice draft from submarine cruises over the Arctic Ocean shows that there has been a decrease of 1.25 m in ice thickness during the period between 1975 and 2000 (Rothrock et al. 2008), it is not readily apparent from our short record that there is a decrease in annual ice volume exiting Fram Strait. In total, nearly three times the area of the Arctic Ocean is exported over the 29 years (assuming Arctic Ocean area to be ~7.2×10^6 km^2). Taking the mean volume export to be 2200 km^3 yr^{-1}, sea ice with thicknesses of approximately 9 m was exported during the same period. Recent variability in sea ice export is associated with the atmospheric indexes; the squared correlation between the DJFM Fram Strait area export and NAO indices is 0.36, and it is 0.28 for the AO, slightly lower than that reported using shorter records.

The outflows during recent summers (in 2005 and 2007) have been remarkably high. Though the ice flux over the summer of 2005 (144×10^3 km^2) was high, the flux in 2007, at 167×10^3 km^2 (2σ from the mean), was the highest on record and accounted for over 20% of the 2006–07 annual area Arctic outflow. As noted by Kwok (2007), the consequence of summer ice export is different from that of the winter. During the winter or growth season, the sea ice area (especially multiyear ice) depleted by export is replaced by seasonal ice. Depending on the winter conditions, these seasonal ice areas have an opportunity to grow and thus a chance to survive the subsequent summer and contribute to the replenishment of the multiyear ice reservoir. This is not the case for ice area exported during the summer. Since there is no freezing of the vacated areas, summer export contributes directly to open water production and the depletion of sea ice area. From an ice area survival perspective, for a given net annual ice export, it would be better to have the higher ice export during the early winter than during the summer. For the 2005 summer, Arctic ice export was directly responsible for ~40% of the ~0.6×10^6 km^2 of decrease in multiyear coverage. Thus, if the changes in the atmospheric circulation are considered a trigger of the unprecedented ice retreat in summer 2007, then the ice albedo feedback accelerated the retreat (Zhang et al. 2008). The large loss of ice mass and ice extent may suggest that Arctic sea ice has entered a state of being particularly vulnerable to anomalous atmospheric forcing.

Although there is no discernible linear trend in strength and orientation of the Transpolar Drift Stream (TDS), it is interesting to note the extremes in these two TDS attributes within the 10-yr period between 1987 and 1996. During this period, there are 5 yr where the net annual displacements of ice particles within the TDS are more than one standard deviation above the mean. This indicates a high ice flux period with orientations of the TDS axis that favor the drainage of sea ice from the western Arctic Ocean and north of Greenland, that is, export of thicker sea ice. As expected, these are the same years when there is a significant advection of sea ice from the Pacific to the Atlantic sector of the Arctic Ocean. During this same period, there are 5 yr where

the net outflow is $>1\sigma$ above the mean, favoring the export of sea ice into the Atlantic sector. Significantly, the increase in sea ice inflow into the Atlantic sector during summer, at a rate of 10.6×10^3 km^2 yr^{-1}, is high; this contributes to over 80% of the annual trend in the exchanges between these sectors (Fig. 11b). Over the 29 years, this trend suggests a remarkable increase from a mean exchange of near zero to an export of more than 300×10^3 km^2 of sea ice to the A sector during the summer. This is associated with an observable change in the summer sea ice circulation and sea level pressure distribution. While the recent winter circulation and SLP have nearly reverted to conditions typical of the 1980s, the summer IM and SLP have not. Compared to the 1980s, the recent SLP distributions show much lower pressures (2–3 hPa) over much of the Arctic. Overall, since the 1980s there has been a strengthening of the summer TDS. As discussed above, this creates more open water, reduces the survivability of the ice cover, and lowers the ice volume/storage in the Pacific sector. This also suggests that, because of the advection of sea ice into the A sector in summer, the summer ice extent in this sector has remained relatively stable compared to that in the Pacific sector. It is highly likely that these decadal changes in summer circulation could partly explain the recent record minimums in summer ice coverage in the Pacific sector while the Atlantic sector coverage has remained unchanged. This also alters our notion of relatively weak SLP gradients during the summer months.

The net Arctic sea ice outflows into the Barents Sea are small and are dwarfed by that at Fram Strait. The net annual outflow at the S–FJL passage is $37(39) \times 10^3$ km^2. The large outflow of multiyear ice in 2002–03, marked by an area and volume outflow of 141×10^3 km^2 and $\sim$300 km^3, was unusual across the record. There is a mean annual inflow of seasonal ice through the FJL–SZ passage of $103\ (93) \times 10^3$ km^2. The source of this sea ice is the Barents as well as the Kara Sea. Although the mean flux is small, there could be unusual conditions periodically (as in 2002–03 at the S–FJL) that lead to anomalously high ice export.

Acknowledgments. I wish to thank S. S. Pang at JPL for her software support during the preparation of this manuscript. The SMMR, SSM/I, and AMSR-E brightness temperature and ice concentration fields are provided by World Data Center A for Glaciology/National Snow and Ice Data Center, University of Colorado, Boulder, Colorado. This work was carried out at the Jet Propulsion Laboratory, California Institute of Technology, and is sponsored by the National Science Foundation and the National Aeronautics and Space Administration.

REFERENCES

Aagaard, K., and E. C. Carmack, 1989: The role of sea ice and other fresh waters in the Arctic circulation. *J. Geophys. Res.,* **94** (C10), 14 485–14 498.

——, and R. A. Woodgate, 2001: Some thoughts on the freezing and melting of sea ice and their effects on the ocean. *Ocean Modell.,* **3,** 127–135.

Belkin, I. M., S. Levitus, J. Antonov, and S.-A. Malmberg, 1998: ''Great Salinity Anomalies'' in the North Atlantic. *Prog. Oceanogr.,* **41,** 1–68.

Cavalieri, D. J., 1992: The validation of geophysical products using multisensor data. *Microwave Remote Sensing of Sea Ice, Geophys. Monogr.*, Vol. 68, Amer. Geophys. Union, 233–242.

Comiso, J. C., 2002: A rapidly declining perennial sea ice cover in the Arctic. *Geophys. Res. Lett.,* **29,** 1956, doi:10.1029/2002GL015650.

——, and F. Nishio, 2008: Trends in the sea ice cover using enhanced and compatible AMSR-E, SSM/I, and SMMR data. *J. Geophys. Res.,* **113,** C02S07, doi:10.1029/2007JC004257.

——, C. L. Parkinson, R. Gersten, and L. Stock, 2008: Accelerated decline in the Arctic sea ice cover. *Geophys. Res. Lett.,* **35,** L01703, doi:10.1029/2007GL031972.

Curry, R., and C. Mauritzen, 2005: Dilution of the northern North Atlantic Ocean in recent decades. *Science,* **208,** 1772–1774.

——, B. Dickson, and I. Yashayaev, 2003: A change in the freshwater balance of the Atlantic Ocean over the past four decades. *Nature,* **426,** 826–829.

Dickson, R. R., J. Meincke, S. A. Malmberg, and J. Lee, 1988: The ''Great Salinity Anomaly'' in the northern North Atlantic 1968-1982. *Prog. Oceanogr.,* **20,** 103–151.

Gascard, J.-C., and Coauthors, 2008: Exploring Arctic transpolar drift during dramatic sea ice retreat. *Eos, Trans. Amer. Geophys. Union,* **89,** 150, doi:10.1029/2008EO030001.

Hilmer, M., and T. Jung, 2000: Evidence for a recent change in the link between North Atlantic Oscillation and Arctic sea ice export. *Geophys. Res. Lett.,* **27,** 989–992.

Hurrell, J. W., 1995: Decadal trends in the North Atlantic Oscillation: Regional temperatures and precipitation. *Science,* **269,** 676–679.

Kwok, R., 2000: Recent changes of the Arctic Ocean sea ice motion associated with the North Atlantic Oscillation. *Geophys. Res. Lett.,* **27,** 775–778.

——, 2007: Near zero replenishment of the Arctic multiyear sea ice cover at the end of 2005 summer. *Geophys. Res. Lett.,* **34,** L05501, doi:10.1029/2006GL028737.

——, 2008: Summer sea ice motion from the 18 GHz channel of AMSR-E and the exchange of sea ice between the Pacific and Atlantic sectors. *Geophys. Res. Lett.,* **35,** L03504, doi:10.1029/2007GL032692.

——, and D. A. Rothrock, 1999: Variability of Fram Strait ice flux and North Atlantic Oscillation. *J. Geophys. Res.,* **104** (C3), 5177–5189.

——, and G. F. Cunningham, 2008: ICESat over Arctic sea ice: Estimation of snow depth and ice thickness. *J. Geophys. Res.,* **113,** C08010, doi:10.1029/2008JC004753.

——, ——, and S. S. Pang, 2004: Fram Strait sea ice outflow. *J. Geophys. Res.,* **109,** C01009, doi:10.1029/2003JC001785.

——, W. Maslowski, and S. W. Laxon, 2005: On large outflows of Arctic sea ice into the Barents Sea. *Geophys. Res. Lett.,* **32,** L22503, doi:10.1029/2005GL024485.

Lindsay, R. W., and J. Zhang, 2005: The thinning of Arctic sea ice, 1988–2003: Have we reached the tipping point? *J. Climate,* **18,** 4879–4895.

Maslanik, J., and J. Stroeve, cited 2007: DMSP SSM/I daily polar gridded brightness temperatures. National Snow and Ice Data Center. [Available online at http://nsidc.org/data/amsre/data_summaries.html.]

Morison, J., J. Wahr, R. Kwok, and C. Peralta-Ferriz, 2007: Recent trends in Arctic Ocean mass distribution revealed by GRACE. *Geophys. Res. Lett.,* **34,** L07602, doi:10.1029/2006GL029016.

Parkinson, C. L., and D. J. Cavalieri, 2008: Arctic sea ice variability and trends, 1979–2006. *J. Geophys. Res.,* **113,** C07003, doi:10.1029/2007JC004558.

Peterson, B. J., J. McClelland, R. Curry, R. M. Holmes, J. E. Walsh, and K. Aagaard, 2006: Trajectory shifts in the Arctic and subarctic freshwater cycle. *Science,* **313,** 1061–1066.

Rigor, I. G., J. M. Wallace, and R. L. Colony, 2002: Response of sea ice to the Arctic Oscillation. *J. Climate,* **15,** 2648–2663.

Rothrock, D. A., D. B. Percival, and M. Wensnahan, 2008: The decline in arctic sea-ice thickness: Separating the spatial, annual, and interannual variability in a quarter century of submarine data. *J. Geophys. Res.,* **113,** C05003, doi:10.1029/2007JC004252.

Serreze, M. C., and Coauthors, 2006: The large-scale freshwater cycle of the Arctic. *J. Geophys. Res.,* **111,** C11010, doi:10.1029/2005JC003424.

Steele, M., D. Thomas, D. Rothrock, and S. Martin, 1996: A simple model study of the Arctic Ocean freshwater balance, 1979–1985. *J. Geophys. Res.,* **101,** 20 833–20 848.

Thompson, D. W. J., and J. M. Wallace, 1998: The Arctic Oscillation signature in the wintertime geopotential height and temperature fields. *Geophys. Res. Lett.,* **25,** 1297–1300.

Vinje, T., 2001: Fram Strait ice fluxes and atmospheric circulation: 1950–2000. *J. Climate,* **14,** 3508–3517.

Woodgate, R. A., K. Aagaard, R. D. Muench, J. Gunn, G. Bjork, B. Rudels, A. T. Roach, and U. Schauer, 2001: The Arctic Ocean boundary current along the Eurasian slope and the adjacent Lomonosov Ridge: Water mass properties, transports and transformations from moored instruments. *Deep-Sea Res. I,* **48,** 1757–1792.

Zhang, J., R. Lindsay, M. Steele, and A. Schweiger, 2008: What drove the dramatic retreat of arctic sea ice during summer 2007? *Geophys. Res. Lett.,* **35,** L11505, doi:10.1029/2008GL034005.